

Elektrostatik Sprey Kaplama (ESD) Metodu ile Zirkonya ve CGO (Seryum Gadolinium Oksit) Üzerine $La_{1-x}Sr_xCo_{1-y}Fe_yO_{3-\delta}$ Filmlerinin Kaplanması

Hande BÜYÜKKEBABÇI¹, Sedat AKKURT²

¹ İzmir Yüksek Teknoloji Enstitüsü, Mühendislik Fakültesi, Malzeme Bilimi ve Mühendisliği Bölümü, İzmir.

² İzmir Yüksek Teknoloji Enstitüsü, Mühendislik Fakültesi, Makina Mühendisliği Bölümü, İzmir.

e-posta: handebuyukkebabci@gmail.com

Geliş Tarihi:22.10.2012; Kabul Tarihi: 11.11.2013

Özet

Bu çalışmada $La_{0.6}Sr_{0.4}Co_{0.8}Fe_{0.2}O_{3-\delta}$ ve $La_{0.6}Sr_{0.4}Co_{0.2}Fe_{0.8}O_{3-\delta}$ katot malzemelerinin TZ-3Y (%3 mol yitriya katkılı zirkonya) ve CGO seramik elektrolitlerinin üzerine kaplanmasının karakterizasyonu çalışılmıştır. Orta sıcaklıktaki katı oksit yakıt hüçelerine uyumlu katot ve elektrolit malzemesini geliştirebilmek için elektrostatik sprej kaplama tekniği kullanılmıştır. Çeşitli metalik tuzlar kullanılarak $La_{0.6}Sr_{0.4}Co_{0.8}Fe_{0.2}O_{3-\delta}$ veya $La_{0.6}Sr_{0.4}Co_{0.2}Fe_{0.8}O_{3-\delta}$ stokiometrilere sahip çözeltiler hazırlanmıştır. Bu çözeltiler, sıcak seramik yüzey üzerine püskürtülmüş ve böylece seramik yüzey kaplanmıştır. Çözeltinin akış oranı (0.3-1.5 ml/s), püskürtücü ile seramik yüzey arasındaki uzaklık (15-45 mm), substrat sıcaklığı (250-375°C), kaplanmış yüzeylerin sıcaklığı (900-1300°C) ve uygulanan voltaj gibi deneysel parametrelerin kaplama kalitesi üzerine etkileri, DTA/TGA, taramalı elektron mikroskobu (SEM) ve X ışınları analizi (XRD) kullanılarak incelenmiştir. Kaplanan mikroyapılar, kaplama parametrelerine bağlı olarak yoğun ve poroz şeklinde çeşitlendirilmiştir. En iyi ağ mikroyapı, 30 mm uzaklık ve 0.7 ml/s akış oranında sahip olan örnekte elde edilmiştir. Tanelerin üst üste binme etkisi hiçbir numunede gözlenmemiştir. TZ-Y3 seramik yüzeyi $La_{0.6}Sr_{0.4}Co_{0.8}Fe_{0.2}O_{3-\delta}$ ve $La_{0.6}Sr_{0.4}Co_{0.2}Fe_{0.8}O_{3-\delta}$ katot üretimi için kullanışlı değilken, seryum gadolinium oksit seramik yüzey ise sadece $La_{0.6}Sr_{0.4}Co_{0.8}Fe_{0.2}O_{3-\delta}$ katot malzeme üretimi için kullanışlıdır.

Anahtar kelimeler

Elektrostatik Sprej,
Kaplama; Katı Oksit,
Yakıt Pilleri;
 $La_{1-x}Sr_xCo_{1-y}Fe_yO_{3-\delta}$;
Seryum Gadolinium
Oksit.

Coating of $La_{1-x}Sr_xCo_{1-y}Fe_yO_{3-\delta}$ Films on Zirconia and CGO (Cerium Gadolinium Oxide) by Electrostatic Spray Deposition (ESD)

Abstract

In this study preparation and characterization of coating of $La_{0.6}Sr_{0.4}Co_{0.8}Fe_{0.2}O_{3-\delta}$ and $La_{0.6}Sr_{0.4}Co_{0.2}Fe_{0.8}O_{3-\delta}$ materials on TZ-3Y (3 mol % doped yttria) and CGO ($Ce_{0.9}Gd_{0.1}$ Oxide) ceramic electrolytes was studied. Electrostatic spray deposition (ESD) was used for depositing the coatings on ceramic electrolytes to develop a well bonded electrolyte-cathode material for potential IT-SOFCs (intermediate temperature solid oxide fuel cells) applications. Precursor solutions having $La_{0.6}Sr_{0.4}Co_{0.8}Fe_{0.2}O_{3-\delta}$ or $La_{0.6}Sr_{0.4}Co_{0.2}Fe_{0.8}O_{3-\delta}$ stoichiometry were prepared from various salts before being sprayed on a heated ceramic substrate which rapidly evaporated the solvent in the salts and covered its surface. Effects of experimental parameters like the flow rate of the solution (0.3-1.5 ml/h), distance between the nozzle and substrate (15-45 mm), temperature of the substrate (250-375 °C), post heat treatment temperature (900-1300 °C) of the coated substrate and applied voltage on the quality of the coating were studied by several methods including DTA/TGA, Scanning Electron Microscopy (SEM) and X-ray Diffraction (XRD). Coating microstructures ranged from dense to porous depending on the deposition parameters. Sample with 30 mm distance and 0.7 ml/h of flow rate produced the best reticulated structure of the coating. No preferential landing effect was observed on any of the samples studied. Zirconia was not an effective substrate for formation of $La_{0.6}Sr_{0.4}Co_{0.8}Fe_{0.2}O_{3-\delta}$ or $La_{0.6}Sr_{0.4}Co_{0.2}Fe_{0.8}O_{3-\delta}$. Cerium gadolinium oxide, however, was effective for $La_{0.6}Sr_{0.4}Co_{0.8}Fe_{0.2}O_{3-\delta}$ but not for $La_{0.6}Sr_{0.4}Co_{0.2}Fe_{0.8}O_{3-\delta}$.

Key words

Electrostatic Spray
Deposition; Solid
Oxide
Fuel Cells; $La_{1-x}Sr_xCo_{1-y}Fe_yO_{3-\delta}$; Cerium
Gadolinium Oxide.

1. Introduction

Fuel cells can generate energy from fossil fuels more efficiently and more benignly than other alternatives. A fuel cell is an electrochemical cell, which can convert the chemical energy of a fuel and an oxidant to electrical energy by a process involving electrode-electrolyte system without combustion of the fuel at high temperature. Hence, no environmentally hazardous emissions are produced. Moreover, effective, clean, modular and reliable nature of fuel cells make them interesting candidates for energy generation. The basic operating principle of fuel cells were demonstrated in 1839 (Hoogers et al. 2003). A Solid Oxide Fuel Cell (SOFC) is typically composed of two porous electrodes (anode and cathode) interposed between them is an electrolyte made of a dense solid oxide ceramic material. The cathode and anode electrodes show electronic and ionic conductivity (Huijmans et al. 2001). The electrolyte in this fuel cell is a solid, nonporous metal oxide; usually Y_2O_3 stabilized ZrO_2 (YSZ). The cell operates at around 1000°C where ionic conduction by oxygen ions takes place. Typically, the anode is Ni- ZrO_2 cermet and the cathode is Sr doped LaMnO_3 (LSM) (EG&G Technical Services, 2004).

Some important properties are expected from fuel cells such as high conversion efficiency, environmental compatibility and multifuel capability. When these properties are considering, ceramic fuel cells are appropriate devices because they prevent material corrosion and electrolyte management problems. Ceramic fuel cells are defined as SOFCs (Minh et al. 1995).

Energy conversion using SOFCs is a highly efficient and a benign technology for environmental. It reduces the emission of pollutants, such as NO_x , SO_x , CO_2 and dust. However, the development of SOFC for efficient power generation has still failed to reach commercial viability because of high operating temperature SOFCs and due to the long-term degradation problems. Therefore, the development of intermediate-temperature SOFCs (IT-SOFCs) has been started at $500\text{--}700^\circ\text{C}$. Since the operation at intermediate temperatures causes an

increase in the interfacial polarization losses of a solid state cell, as well as ohmic loss in the electrolyte, the performance of IT-SOFCs is strongly dependent on both the electrolyte and the cathode electrolyte interface (Taniguchi et al. 2003). Other one of the most important reasons for lowering the temperature is the reduced cost of the system. Moreover, the use of lower temperature can increase the lifetime of the fuel cell (Marinha et al. 2009). Decreasing the operating temperature leads to increased ohmic losses. To minimize the ohmic drop through the electrolyte research efforts are underway (Wilhelm et al. 2005). The developments of new electrolytes with high ionic conductivity as well as efforts to reduce the thickness of the electrolyte are tested to decrease the ohmic resistance (Steele et al. 2000). Scandia stabilized zirconia (ScSZ) (Yamamoto et al. 1995), TZ-2Y (Nguyen et al. 2001), Cerium gadolinium oxide (CGO) (Taniguchi et al. 2003; Marinha et al. 2009, respectively) are examples for tests on different electrolyte materials in order to minimize the ohmic losses. The cathode material used in the electrode naturally depends on the type of the electrolyte material. Therefore for SOFC material development, the whole system should be considered, not the performance of individual components (Tietz et al. 2008). Significant expertise is built now on the assembly of these components into an SOFC stack which produces the desired power (Ecn, 2010).

Electrostatic spray deposition (ESD) is a modern technique of depositing films on substrates. This process provides many advantages: experimental devices are simple and inexpensive, a wide range of precursor, depositing, a good control of morphology and stoichiometric deposited layers. Moreover, the depositing process can be done under air.

To the best of our knowledge, although the deposition of LSCF cathode material on CGO was investigated earlier (Taniguchi et al. 2003; Marinha et al. 2009). But, preparation and characterization of coating of $\text{La}_{0.6}\text{Sr}_{0.4}\text{Co}_{0.8}\text{Fe}_{0.2}\text{O}_{3-\delta}$ and $\text{La}_{0.6}\text{Sr}_{0.4}\text{Co}_{0.2}\text{Fe}_{0.8}\text{O}_{3-\delta}$ cathode materials on yttria doped 3% mol zirconia (TZ-3Y) and CGO

(Ce_{0.9}Gd_{0.1}Oxide) ceramic electrolytes were analyzed and compared, for the first time. Furthermore, after coating of La_{1-x}Sr_xCo_{1-y}Fe_yO_{3-δ} films on zirconia and CGO by ESD was successfully achieved, the flow rate of the solution, distance between the nozzle and substrate, temperature of the substrate, post heat treatment temperature of the coated substrate and applied voltage on the quality of the coating were studied by DTA/TGA, SEM and XRD in details

2. Experimental

2.1. Materials

For the purpose of the substrate of ceramic electrolyte discs preparation, cerium gadolinium oxide (Ce_{0.9}Gd_{0.1}Oxide, PRAXAIR, 99.9%) and zirconia TZ-3Y (doped with 3 mol. % Y₂O₃, TOSOH, 99.9%) were used.

Precursor solutions for coating of cathode were prepared from mixtures of lanthanum nitrate, hexahydrate (RECTAPUR, 99.99%), iron III nitrate, nonahydrate (SIGMA-ALDRICH, 99.99%), cobalt II nitrate, hexahydrate (SIGMA-ALDRICH, 99.999%) and strontium chloride hexahydrate (STREM CHEMICALS, 99%) salts. The solvents used for dissolving these salts were either ethanol (SIGMAALDRICH, 99.8%) in water or diethylene glycol monobutyl ether (butyl carbitol, ACROS ORGANICS, 99+%)

2.2. Methods

2.2.1. Preparation of the Substrate

The CGO powders to be used for pellet preparation were first calcined (Carbolite Furnace HTC 1000) at 700°C for 7 h. TZ-3Y and CGO powders were compacted by uniaxial pressing in a stainless steel die (Φ= 22.7mm) at 1000 kgf, then by CIP (Cold Isostatic Pressing) at 250 MPa. Samples were placed in a plastic bag under vacuum to avoid penetration of oil during the CIP process. The samples were sintered (Carbolite Furnace HTC 1500) at 1400°C and 1450°C for 2 and 4 hours in air, respectively. Heating rates were 1.6 and 5°C/min respectively. The surfaces of all densified substrates were machined to produce a straight polished surface. 6 μm, 3 μm and 0.2 μm diamond suspensions were used in polishing to obtain uniform surface (Presi, Mecapol 200). Finally, samples around 19 mm of diameter and 1.2 mm of thickness, were obtained. These samples were then ready for ESD coating process.

2.2.2. Preparation of Precursor Solutions for Cathode

A solution is sprayed up through a nozzle on the heated ceramic substrate. This solution is prepared from different salts to produce the final desired stoichiometry of the cathode. The weight of the precursor salt for a particular component *i* is defined as *m_i* and is diluted in the solvent as determined using the following equation:

$$m_i = x_i \cdot M_i \cdot C \cdot V \text{ (Equation 1)}$$

x_i: atomic fraction

M_i: molecular weight

C: concentration of solution (mol/L)

V: solution volume (L)

La(NO₃)₃·6H₂O, SrCl₂·6H₂O, Fe(NO₃)₃·9H₂O, Co(NO₃)₂·6H₂O were used as precursor salts. Ethanol (C₂H₅OH, SIGMA-ALDRICH), diethylene glycol monobutyl ether also known as butyl carbitol ((CH₃(CH₂)₃OCH₂-CH₂OCH₂CH₂OH, ACROS) and H₂O were used as solvents. These salts were mixed in different proportions as listed in Table 1. In this table, solution names coded as ratio of cobalt to iron and ethanol, H₂O and butyl carbitol, respectively. Total salt concentration was 0.02mol/L. Solution names are given by using the first digits of their cobalt and iron percentages as well as their ethanol, water and butyl carbitol contents.

Table 1. Proportion of salts and solvent for all solutions. Amounts of lanthanum nitrate and strontium chloride were constant

Solution Name	Cobalt	Iron	Ethanol	H ₂ O	Butyl carbitol	Conductivity (mS/cm)
82-820	80	20	80	20	0	1.085
28-820	20	80	80.0	20	0	1.749
82-306	80	20	33.3	0	66.7	0.041
28-306	20	80	33.3	0	66.7	0.050

2.2.3. Experimental Setup

All LSCF films were deposited using a vertical electrostatic spray deposition (ESD) system located in LEPMI, Grenoble, France. Installation is vertical to avoid the drops and any flow of the precursors solution on the substrate. The experimental setup is used for depositing of the coating is shown in Figure 1.

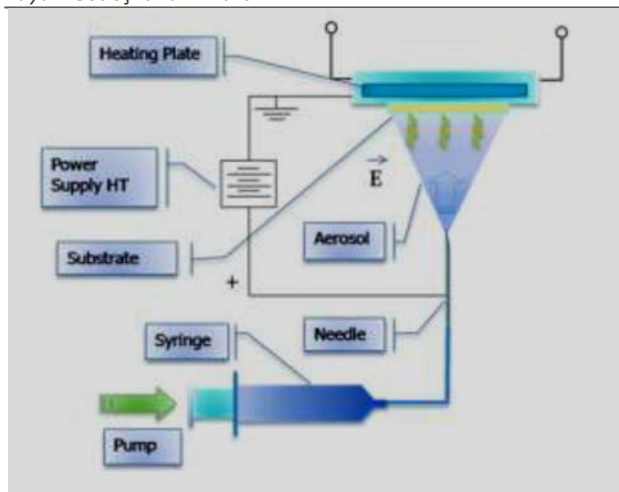


Figure 1. Schematic drawing of the ESD setup used in sample preparation

ESD process consists of:

- i. Electrostatic spray unit
- ii. A liquid precursor feed unit
- iii. Temperature control unit

The electrostatic spray unit comprises a high voltage power supply, a stainless steel nozzle and a grounded substrate holder. The liquid precursor feed unit consists of syringe and a syringe pump (Kd Scientific M361). The temperature control unit for the deposition temperature includes a heating plate and a temperature controller connected to a thermocouple.

When a sample was ready to be deposited, it was placed on the stainless steel holder with a 8 mm hole in the middle to allow sprayed material to coat a small area on the surface of the ceramic. Top side of the ceramic rested against a heating plate. The precursor solution was filled inside a 10 ml syringe (Becton Dickinson) which could be pushed at a controlled speed to deliver the desired amount of solution through the nozzle. A positive high voltage was applied to the stainless steel nozzle while the solution was sprayed. This high voltage produced electrostatically stressed, positively charged conically shaped droplets also known as Taylor cone (Chen, 1998) that were generated and directed to the grounded substrate. Eventually, the surface of the electrolyte ceramic was coated with a thin layer of cathode material. Upon contact with the heated substrate the solvent in the solution rapidly evaporates and an LSCF film with desired stoichiometry forms.

2.2.4. Experimental Plan

Experimental conditions for all samples were listed in Table 2. Two separate ceramic substrates of CGO and TZ-3Y were used and these were dense ceramics that were previously fired to achieve a low porosity substrate before being polished with diamond suspension. Polished samples were coated by an LSCF layer by ESD process. Final stage of processing was post heat treatment of the coated ceramics to achieve a mature ceramic coating.

2.2.5. Characterization

Characterization has a crucial role in interpreting the structure and property relationship between $\text{La}_{0.6}\text{Sr}_{0.4}\text{Co}_{0.8}\text{Fe}_{0.2}\text{O}_{3-\delta}$ and $\text{La}_{0.6}\text{Sr}_{0.4}\text{Co}_{0.2}\text{Fe}_{0.8}\text{O}_{3-\delta}$ on CGO and TZ-3Y. So, X-ray diffraction (XRD, Panalytical Xpert Pro MPD) and scanning electron microscopy (SEM, LEO Stereoscan S440) were utilized for microstructural characterization and thermogravimetric analysis (DTA/TG, Netzsch STA 409) for thermal property characterization.

2.2.5.1. Differential Thermal Analysis (DTA/ TGA)

In order to determine the thermal decomposition temperatures, thermogravimetric analysis (TGA) was performed on $\text{La}_{0.6}\text{Sr}_{0.4}\text{Co}_{0.8}\text{Fe}_{0.2}\text{O}_{3-\delta}$, $\text{La}_{0.6}\text{Sr}_{0.4}\text{Co}_{0.2}\text{Fe}_{0.8}\text{O}_{3-\delta}$ solutions with DTA/TGA (Netzsch STA 409) under ambient atmosphere. Solutions of 100-130 mg were heated from room temperature to 690°C at a heating rate of 10°C/min.

2.2.5.2. Scanning Electron Microscopy

Scanning electron microscope (SEM, LEO Stereoscan S440) was used to investigate the surfaces of LSCF films and for interpreting the porous and dense microstructures.

Table 2. Experimental conditions for all the samples

Sample Code No.	LSCF composition *	Distance (mm)	Flow rate (ml/h)	Deposition Time (h)	Deposition Temperature (°C)	Annealing Temperature (°C)	Solution Name
C1	6482	15	0.3	1	250	900	82-820
C2	6482	30	0.3	1	250	900	82-820
C3	6482	45	0.3	1	250	900	82-820
C4	6482	15	0.7	1	250	900	82-820
C5	6482	30	0.7	1	250	900	82-820
C6	6482	45	0.7	1	250	900	82-820
C7	6482	15	1.5	1	250	900	82-820
C8	6482	30	1.5	1	250	900	82-820
C9	6482	45	1.5	1	250	900	82-820
C10	6482	35	1.0	1	300	900	82-820
C11	6482	35	1.0	1	350	900	82-820
C12	6482	35	1.0	1	375	900	82-820
C13	6482	35	1.0	5	350	900	82-306
C14	6482	35	1.0	5	350	1100	82-306
C15	6482	35	1.0	5	350	1300	82-306
C16	6428	35	1.0	5	350	900	28-306
C17	6428	35	1.0	5	350	1100	28-306
C18	6428	35	1.0	5	350	1300	28-306
Z1	6482	35	1.0	5	350	900	82-306
Z2	6482	35	1.0	5	350	1100	82-306
Z3	6482	35	1.0	5	350	1300	82-306
Z4	6428	35	1.0	5	350	900	28-306
Z5	6428	35	1.0	5	350	1100	28-306
Z6	6428	35	1.0	5	350	1300	28-306
RC4	6428	15	0.7	1	250	900	28-306

2.2.5.3. X-Ray Diffraction Analysis

X-ray diffraction analysis (XRD) was performed using a PANalytical X'Pert Pro MPD diffractometer in the Bragg–Brentano geometry from 10° to 120° , step size and step time were 0.017° and 241.3 sec, respectively.

3. Results and Discussion

3.1. Differential Thermal Analysis (DTA/ TGA) Results

Two types of LSCF solutions with $\text{La}_{0.6}\text{Sr}_{0.4}\text{Co}_{0.8}\text{Fe}_{0.2}\text{O}_{3-\delta}$ and $\text{La}_{0.6}\text{Sr}_{0.4}\text{Co}_{0.2}\text{Fe}_{0.8}\text{O}_{3-\delta}$, stoichiometry were prepared by dissolving their precursor salts in three different solvents (water, ethanol and butyl carbitol). In Figure 2, the three

different solvent mixture compositions are marked on a triangular plot to show the ratio of ethanol, butyl carbitol and water.

DTA/TGA analyses were performed on all of the solutions mentioned to study their thermal behavior. The temperature range for the measurements ranged from room temperature to 690°C at 10°C/min in air. The resulting graphs are shown in Figures 2 to 5. In Figure 3, an endothermic peak at 118°C was observed due to the evaporation of the solvent for the 82-820 and 28-820 samples. The evaporation temperature of H_2O is 100°C while that of ethanol is 78°C. TGA analyses results in Figure 4 also confirmed the DTA observations.

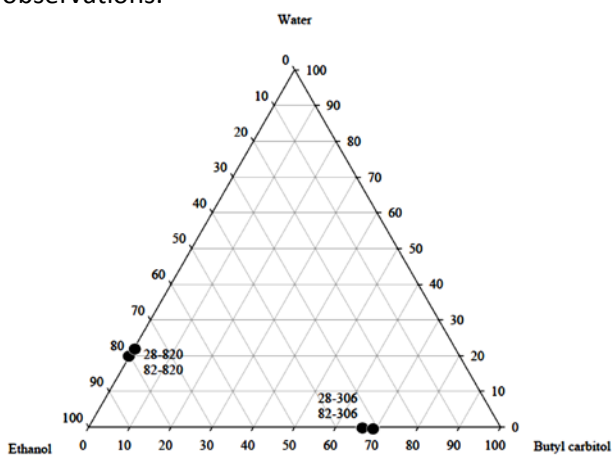


Figure 2. The mixtures prepared from three solvents

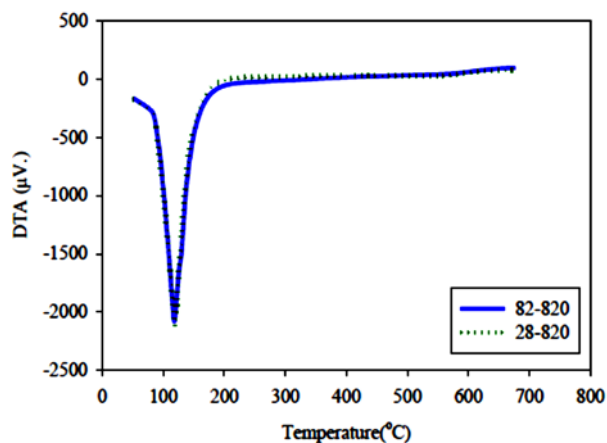


Figure 3. DTA analyses of 82-820 and 28-820 solutions performed under atmospheric conditions at a heating rate of 10°C/min.

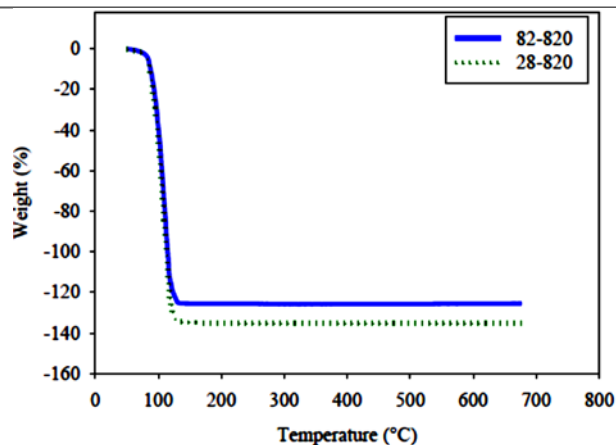


Figure 4. TGA analyses of 82-820 and 28-820 solutions performed under atmospheric conditions at a heating rate of 10°C/min.

In Figure 5, DTA analyses results for solutions with mixtures of ethanol and butyl carbitol were presented. There were two main endothermic peaks at 136°C and 245°C corresponding to the evaporation of ethanol and butyl carbitol, respectively. The former evaporated at a range of temperatures of 95°C to 210°C while the evaporation temperature range for butyl carbitol was narrower. A narrow evaporation temperature range may be helpful for formation of solid crust on ceramic electrolyte. Weight loss as a function of temperature graph (TGA chart in Figure 6) of the solutions further confirmed the DTA observations that butyl carbitol evaporates faster and at higher temperature.

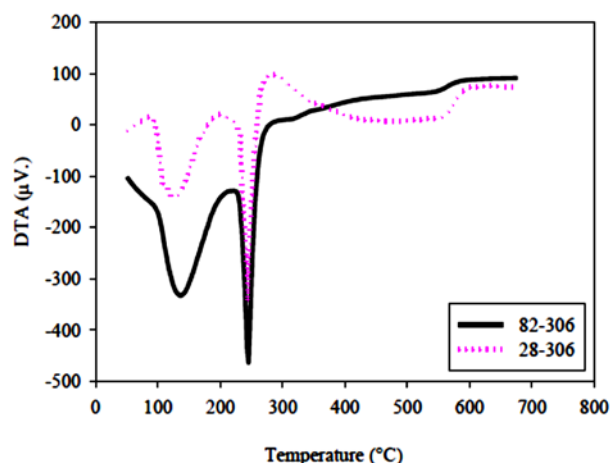


Figure 5. DTA analyses of 82-306 and 28-306 solutions performed under atmospheric conditions at a heating rate of 10°C/min.

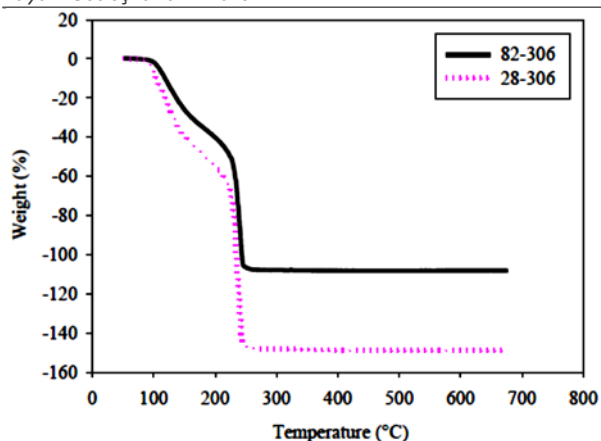


Figure 6. TGA analyses of 82-306 and 28-306 solutions performed under atmospheric conditions at a heating rate of $10^\circ\text{C}/\text{min}$.

3.2. Electrostatic Spray Deposition (ESD) Results The ceramic electrolyte samples were coated with LSCF films using the ESD apparatus as explained in experimental setup. A set of experiments were conducted at 5-15 kV of voltage, 0.3-1.5 ml/hour of solution flow rate, $250\text{-}375^\circ\text{C}$ of heating temperature of the electrolyte and 15-45 mm of nozzle to substrate distance. Coating process was successfully performed without any peeling from the surface.

3.3. Scanning Electron Microscopy (SEM) Results

After the ceramic electrolyte substrates were coated and annealed, their structures were investigated by using Scanning Electron Microscope. Two separate studies were carried out. First, coating surfaces and next the fracture surfaces were observed at high magnification.

To understand the influence of annealing on film morphology, first the CGO substrate was deposited using a flow rate of 1.0 ml/h, nozzle to substrate distance of 35 mm and substrate temperature of 375°C for 2 h. Then, this sample was annealed at 900°C for 2 h. The resulting structure of the coating before and after annealing was compared to find out if film densification increased after annealing because of evaporation of organic residues. The difference of the micrographs can be seen in Figure 7. SEM micrographs taken before and after annealing show that heat treatment in air at 900°C for 2 h. A slight decrease in film thickness due to the film densification and departure of organic residues (Marinha et al., 2009). All remaining samples in this thesis were observed after annealing at 900°C for 2 h

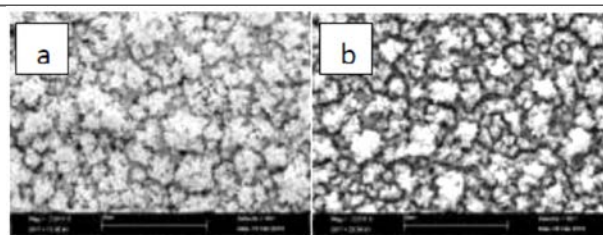


Figure 7. SEM micrographs of the surface of the film, (a) before and (b) after annealing at 900°C for 2 h and applied voltage is 14 kV

LSCF films are observed to investigate the effects of some deposition parameters on the surface morphology of thin films. Properties of LSCF deposits can be modified by changing the following parameters:

- I. nozzle to substrate distances
- II. solution flow rates
- III. deposition temperatures
- IV. heat treatment.

Applied voltage was varied within a narrow margin of 5-15 kV in all experiments. Its effect is expected to be insignificant under the conditions studied in this study.

3.3.1. Influence of Nozzle to Substrate Distance

To study the effect of spraying distance on the morphology of the LSCF films, depositions were carried out at nozzle to substrate distances of 15 mm, 30 mm and 45 mm and flow rates ranged from 0.3 ml/h, 0.7 ml/h and 1.5 ml/h for 1 h at 250°C as shown in Figure 8. According to the first column (C1, C2 and C3), second column (C4, C5 and C6) or third column (C7, C8 and C9), when the distance increases, droplets will be smaller and drier and a very dense microstructure can be obtained, because higher distance will dry up the droplets. It means that, as nozzle to substrate distance increases, deposited particles become increasingly smaller due to larger solvent losses through evaporation occurring during droplet flight. A minor amount of evaporative cooling between the nozzle and the substrate can be expected (Marinha et al., 2009)

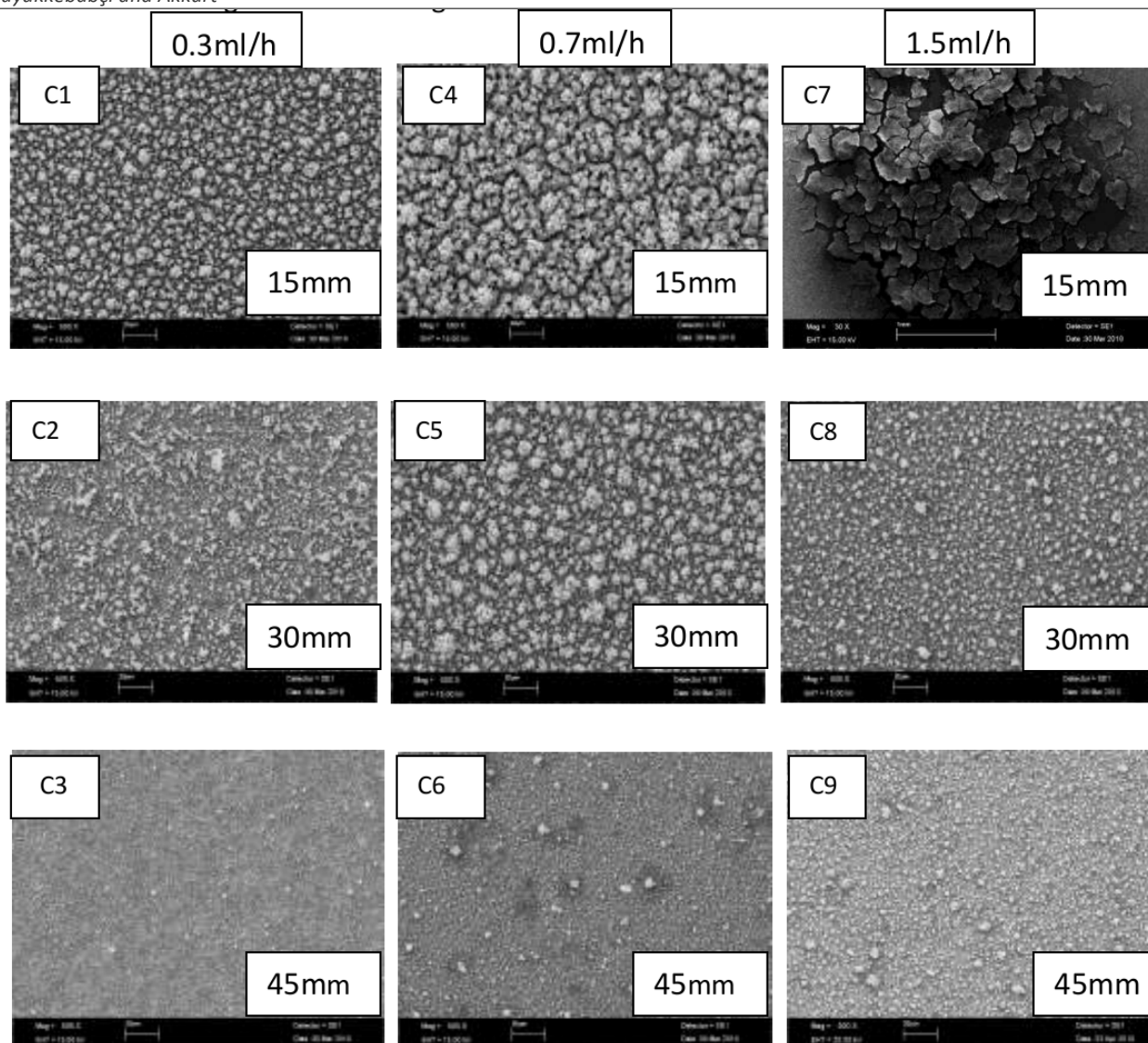


Figure 8. SEM micrographs of $\text{La}_{0.6}\text{Sr}_{0.4}\text{Co}_{0.8}\text{Fe}_{0.2}\text{O}_{3-\delta}$ films deposited on CGO substrate using three different flow rates of 0.3 ml/h, 0.7 ml/h and 1.5 ml/h for 1 h and at a constant temperature 250°C for three different nozzle to substrate distances of 15 mm (first line), 30 mm (second line) and 45 mm (last line). Applied voltage was kept constant at 14 kV

The proportions of the elements displayed by EDS results helped to be sure to identify $\text{La}_{0.6}\text{Sr}_{0.4}\text{Co}_{0.8}\text{Fe}_{0.2}\text{O}_{3-\delta}$ and $\text{La}_{0.6}\text{Sr}_{0.4}\text{Co}_{0.2}\text{Fe}_{0.8}\text{O}_{3-\delta}$ films on the CGO and TZ-3Y substrates (Figures 9, 10, Tables 3, 4). The observed compositions of prepared films are also shown to be in moderately good agreement with the starting solutions. Some Ce and Gd also showed up in EDS measurements but these are removed in this table to facilitate better comparison with theoretical data.

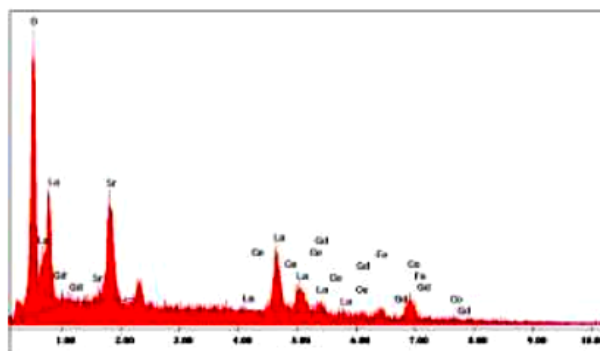


Figure 9. EDS analysis of $\text{La}_{0.6}\text{Sr}_{0.4}\text{Co}_{0.8}\text{Fe}_{0.2}\text{O}_{3-\delta}$ on CGO substrate

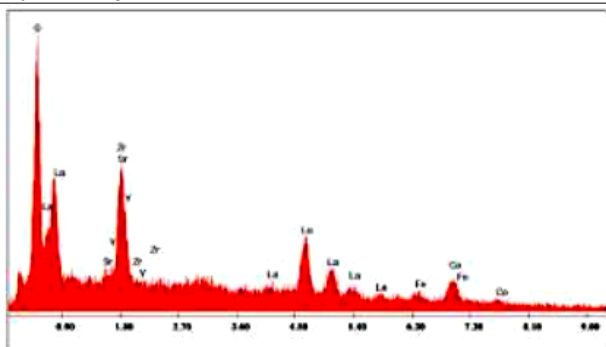


Figure 10. EDS analysis of $\text{La}_{0.6}\text{Sr}_{0.4}\text{Co}_{0.8}\text{Fe}_{0.2}\text{O}_{3-\delta}$ on TZ-3Y substrate

Table 3. EDS analysis results of chemical compositions of $\text{La}_{0.6}\text{Sr}_{0.4}\text{Co}_{0.8}\text{Fe}_{0.2}\text{O}_{3-\delta}$ films

Element (wt%)	EDS analysis wt%	
	Theoretical	Measured
La	37.0	41.9
Sr	15.6	14.2
Co	20.9	24.3
Fe	5.0	6.5
O	Balance	Balance

Table 4. EDS analysis results of chemical compositions of $\text{La}_{0.6}\text{Sr}_{0.4}\text{Co}_{0.2}\text{Fe}_{0.8}\text{O}_{3-\delta}$ films

Element (wt%)	EDS analysis wt%	
	Theoretical	Measured
La	37.4	43.0
Sr	15.7	13.5
Co	5.3	9.2
Fe	20.0	20.5
O	Balance	Balance

3.3.2. Influence of Precursor Solution Flow Rate

When influence of the flow rate is analyzed, higher flow rate will produce larger droplets which are more difficult to dry upon flight, because when the solution flow rate is increased, larger droplets are accumulated and dispatched from the nozzle. Large sized droplets contain more liquid which can take longer flight distances without complete drying. This can be confirmed by comparing the morphology of the films deposited at different flow rates. Microstructures of films deposited using solution flow rates that were varied from 0.3 to 1.5 ml/h are shown in Figures 8 C1-C7, C2-C8 or C3-C9. All photographs in Figure 8, except C7, indicated an

improved reticulated structure upon increased solution flow rates. Sample C7 did not coat well the surface of the substrate because of its excessively high liquid content (Figure 11). As shown in Figure 9, at short distances, many cracks are present at high flow rate because the droplets include larger amounts of solvent which can not find sufficient time to evaporate during their flight.

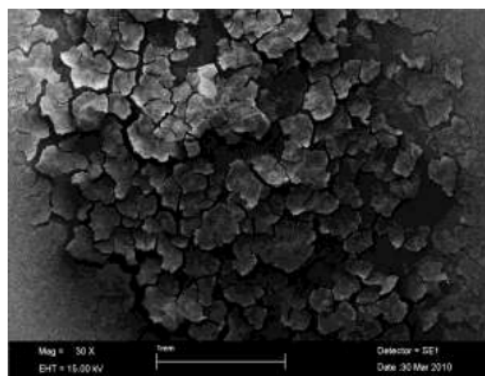


Figure 11. SEM image of the surface of C7 sample of $\text{La}_{0.6}\text{Sr}_{0.4}\text{Co}_{0.8}\text{Fe}_{0.2}\text{O}_{3-\delta}$ layer deposited on a CGO substrate at 0.7 ml/h from a nozzle to substrate distance of 15 mm for 1 h at 250°C and applied voltage is 14 kV

When the samples C3, C6 and C9 are broken and observed from their profiles, the effect of flow rate can be better understood (Figures 12 from a to c). As mentioned before, as the flow rate of precursor solution increased, sprayed droplets increased in size and also increase of layer thickness can be seen, clearly. It is not possible in order to determine microstructure which obtain dense or porous by looking at the microstructure of the flow rate because degree and type of reticulation microstructure depend on a combination of both distance and flow rate.

3.3.3. Influence of Deposition Temperature

Deposition temperature (or the substrate temperature) has an important influence on the quality of coating because it affects the drying rate and the degree of spread of the droplets after impact with the substrate.

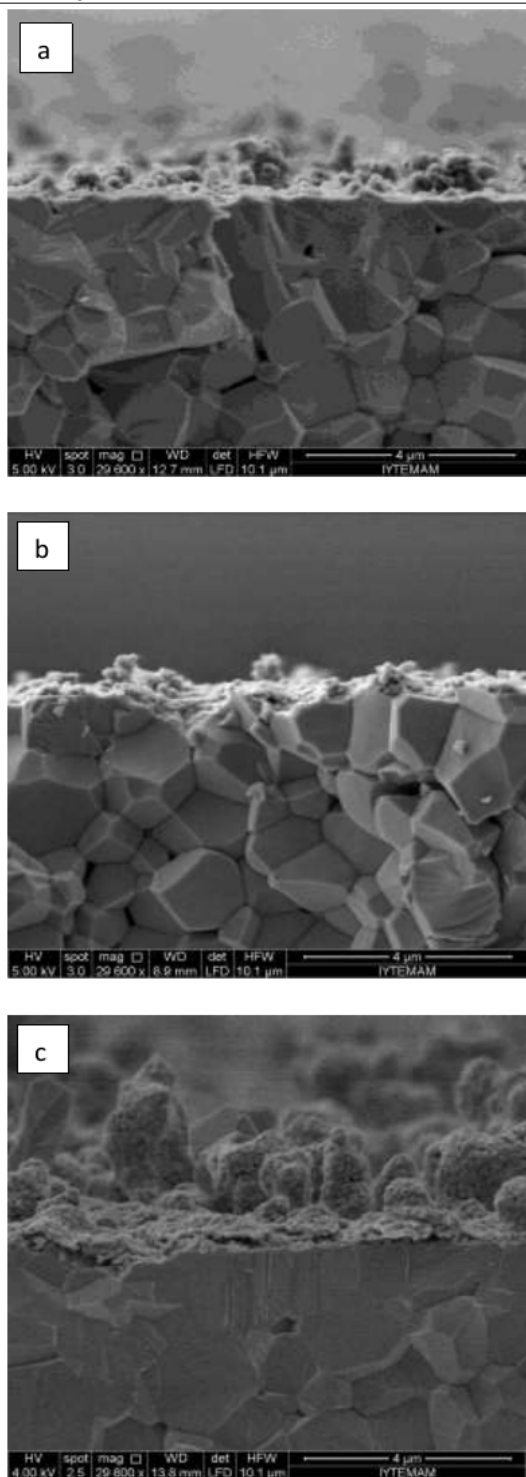


Figure 12. SEM images of the fracture surfaces of $\text{La}_{0.6}\text{Sr}_{0.4}\text{Co}_{0.8}\text{Fe}_{0.2}\text{O}_{3-\delta}$ films deposited on a CGO substrate at (a) 0.3 (b) 0.7 and (c) 1.5 ml/h from a nozzle to substrate distance of 45 mm for 1 h at 250°C (samples C3, C6 and C9) by using 14 kV

It may even be speculated that the drying rate of the droplets during flight depends on the temperature of the substrate. Moreover, obtaining dense or porous microstructure correlates with spreading of the droplets on the surface.

In Figure 13, the effect of substrate temperature (300, 350 and 375°C) on morphology of the deposited films was studied by keeping all other parameters constant. These specimens are coded C10, C11 and C12. As seen in Figure 13, at higher temperatures the droplets dried more and became smaller by producing a more dense structure.

Under the subject of effect of the temperature, preferential landing effect is another important point to mention, because this effect is a determining factor in order to decide if the temperature is too high or not (Marinha et al., 2009). In this study, the temperatures were convenient and preferential landing effect was not observed.

Keeping in mind that the LSCF films are covered on ceramic electrolyte substrates to serve as a cathode layer, the films must be continuous with good reticulated structure to provide the desired electrical conductivity. One may ask what is the best structure for good reticulation. Figure 14 shows a sample (RC4) with good reticulated structure that was obtained with a flow rate of 0.7 ml/h at 250°C at a distance of 15 mm.

3.3.4. Influence of Heat Treatment

In the light of the above mentioned information, in order to see the effect of post annealing heat treatment temperature on the CGO and TZ-3Y microstructures, C13, C14, C15, Z1, Z2 and Z3 tests were conducted by keeping all other experimental conditions constant. The results are shown in Figure 15. At 900°C both CGO and TZ-3Y substrates showed similar microstructures. As the temperature was increased, grain size did not grow significantly, pores closed and surface area appeared to decrease. The coating showed a densified structure due to sintering as the temperature increased.

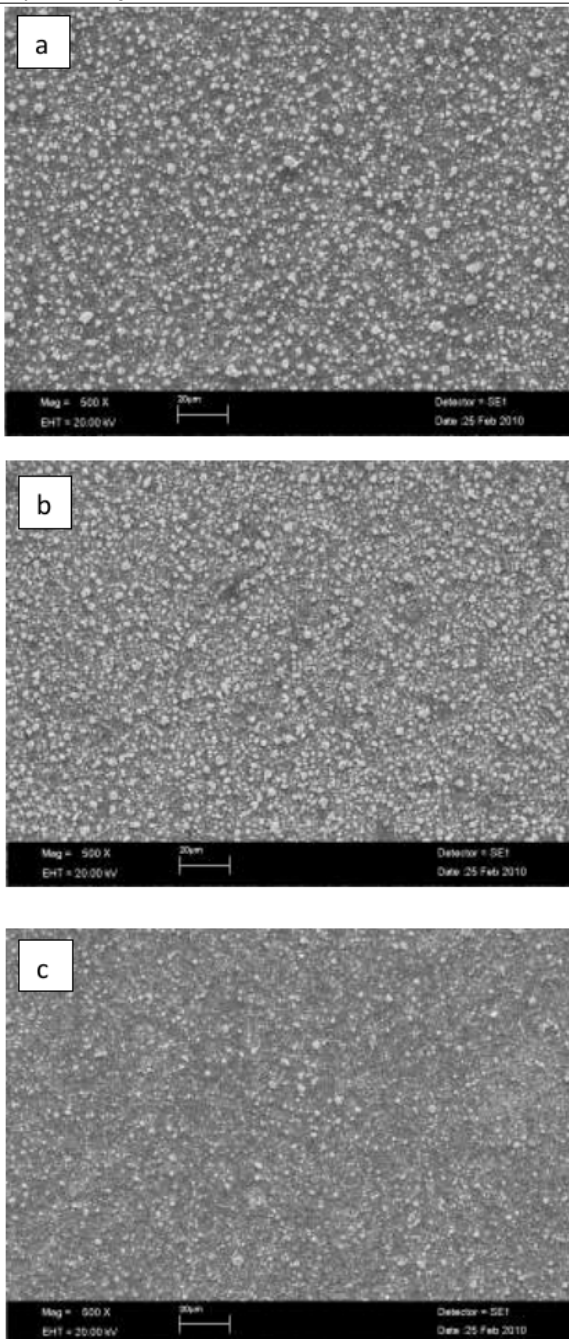


Figure 13. SEM micrographs of $\text{La}_{0.6}\text{Sr}_{0.4}\text{Co}_{0.8}\text{Fe}_{0.2}\text{O}_{3-\delta}$ coated samples of CGO substrates using different temperatures (a) sample C10 at 300°C, (b) sample C11 at 350°C and (c) sample C12 at 375°C. All runs were done at 14 kV

To obtain more detailed information about the quality of coating and the degree of bonding in the samples C13 and Z1, their profile SEM pictures were taken from fracture surfaces of broken sample cross sections. These fracture surfaces are shown in Figures 16 and 17. A crack-free bond was found to form between the substrate and the coating. The coating was porous and continuous with a minimum thickness of roughly 1 µm for both

C13 and Z1 samples which were heat treated at 900°C for 1 hour (Figure 15). C15 and Z3 samples that were heat treated at 1300°C appeared to be highly dense and glassy and were free from pores (Figure 16).

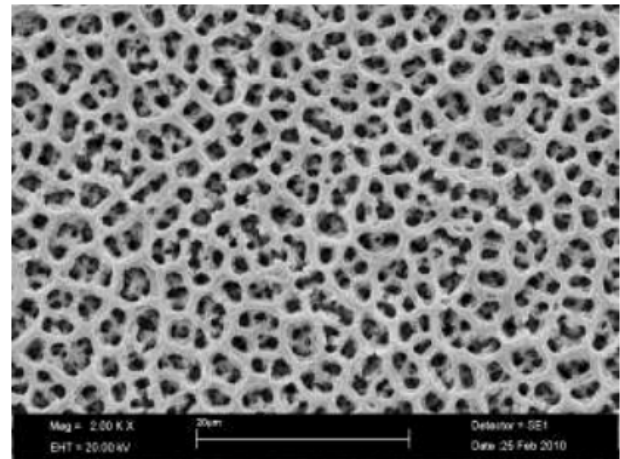


Figure 14. SEM micrographs of sample RC4 showing a well developed reticulated structure by applying 5 kV

Figure 18 shows that the ceramic substrate materials of CGO and TZ-3Y had different grain sizes. Average grain size of CGO sample is obviously larger than the TZ-3Y sample. Average grain sizes of the CGO and TZ-3Y matrices heated at 900 and 1300°C were found to be in the range of 1.75-183 µm and 0.35-0.40 µm, respectively (Figure 18, 19).

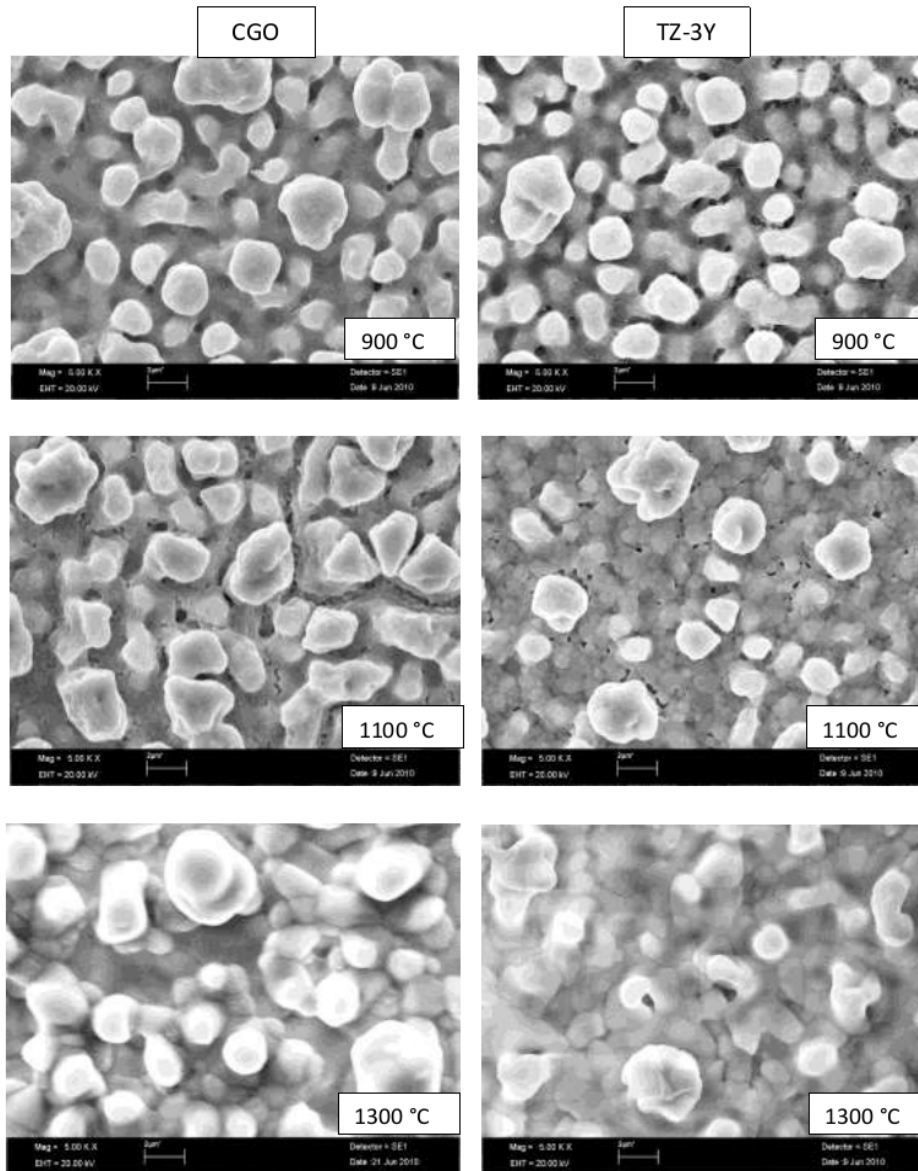


Figure 15. Influence of heat treatment temperature of $\text{La}_{0.6}\text{Sr}_{0.4}\text{Co}_{0.8}\text{Fe}_{0.2}\text{O}_{3-\delta}$ films on CGO (samples C13, C14 and C15 on left column) and TZ-3Y (samples Z1, Z2 and Z3 on right column) by applying 15 kV

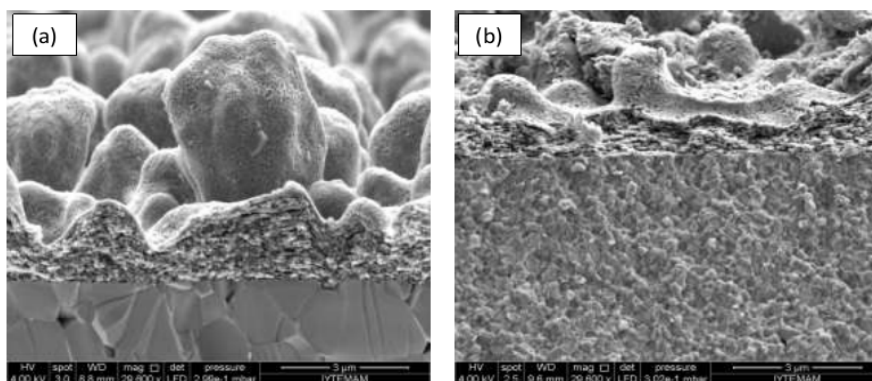


Figure 16. Fracture surfaces of cross sections of (a) sample C13 and (b) sample Z1 coatings that were both annealed at 900 °C

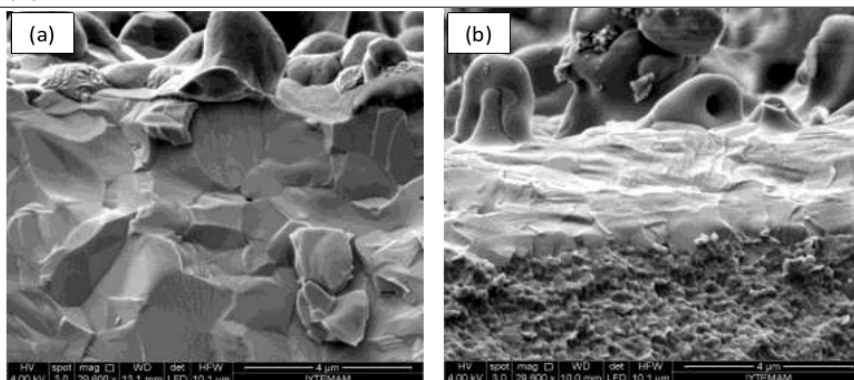


Figure 17. Fracture surfaces of cross sections of (a) sample C15 and (b) sample Z3 coatings that were both annealed at 1300°C. Glassy structure of the coating is evident in both SEM photomicrographs

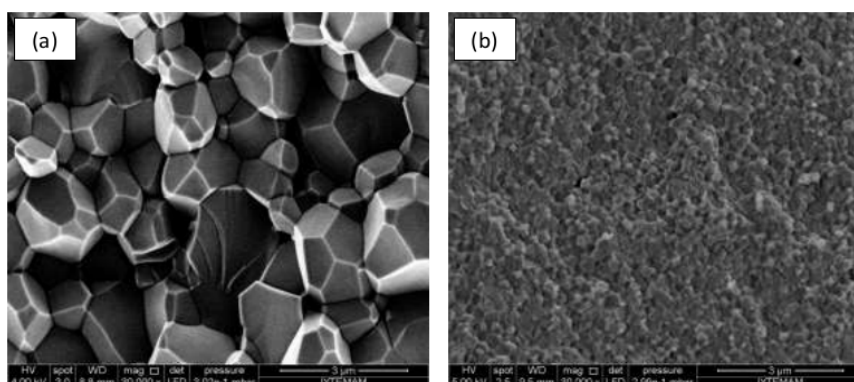


Figure 18. SEM micrographs of fracture surfaces of (a) CGO and (b) TZ-3Y substrates after coating and subsequent thermal treatment at 900°C

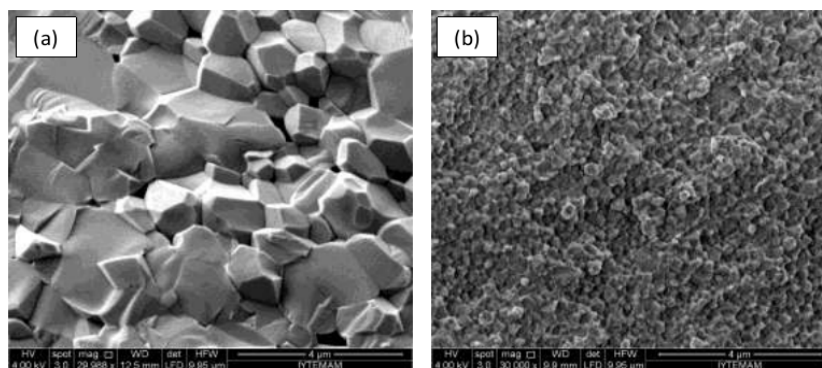


Figure 19. SEM micrographs of fracture surfaces of (a) CGO and (b) TZ-3Y substrates after coating and subsequent thermal treatment at 1300°C

3.4. X-Ray Diffraction Analysis Results

X-ray diffraction analyses were performed to investigate if there is any change caused by the temperature. Figure 20 shows the XRD chart for sample C13 that was heat treated at 900°C. Because the x-ray irradiated area on the specimen surface was larger than the area covered by LSCF coating some peaks from the substrate inevitably appeared on XRD analysis charts. CeO_2 (see also

Table 5) for example, was observed in C13 sample as shown in Figure 20. It is actually the host crystal lattice of the $(\text{Ce}_{0.9}\text{Gd}_{0.1}\text{O})$ CGO compound. Gadolinium is only 10 mol percent of CGO and forms the solute in the solid solution within CeO_2 lattice.

Minor amount of La_2O_3 and LSCF-6491 ($\text{La}_{0.6}\text{Sr}_{0.4}\text{Co}_{0.9}\text{Fe}_{0.1}\text{O}_3$) were also observed. But the observed compound was 6491. Therefore some deviation from expected compositions occurred

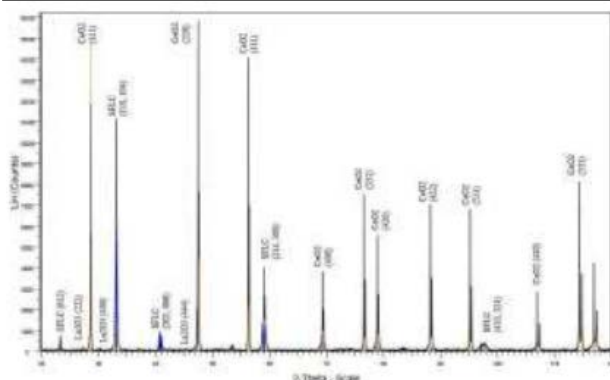


Figure 20. XRD chart for sample C13

Table 5. Phases observed in XRD analysis and their reference card numbers

Compound code used in XRD chart peak labels	Mineral composition	JCPDS reference number
LSCF-6491	$\text{La}_{0.6}\text{Sr}_{0.4}\text{Co}_{0.9}\text{Fe}_{0.1}\text{O}_3$	00-049-0283
CeO ₂	CeO ₂	34-0394
La ₂ O ₃	La ₂ O ₃	03-065-3185
LSCF-6482	$\text{La}_{0.6}\text{Sr}_{0.4}\text{Co}_{0.8}\text{Fe}_{0.2}\text{O}_3$	00-048-0124
ZrO ₂	ZrO ₂	50-1089
LSC	$\text{La}_{0.5}\text{Sr}_{0.5}(\text{CoO}_3)$	01-075-8571
SZO	SrZrO ₃	04-001-7315
LZO	$\text{La}_2(\text{Zr}_2\text{O}_7)$	01-070-5602
LaO	LaO	04-007-4019
LSCF-7337	$\text{La}_{0.7}\text{Sr}_{0.3}\text{Co}_{0.3}\text{Fe}_{0.7}$	01-089-1268
SLF	$\text{Sr}_{0.6}\text{La}_{0.4}\text{FeO}_3$	04-007-6519
LSC	$\text{La}_{0.6}\text{Sr}_{0.4}(\text{CoO}_3)$	01-089-5717

In order to better understand the evolution of the phase composition in the coating samples of CGO were analysed by high temperature XRD (HTXRD) device in Lille University, France. In Figure 21, HTXRD analysis results for sample C13 is given. It should be noted that the post heat treatment was not applied. Peaks from the substrate are obviously observed to slightly shift left toward lower 2θ values. This was expected because of expansion of the lattice as a result of higher atomic vibrations at higher temperatures (Cullity, 1974).

Upon heating of the sample to 500°C and higher LSCF was observed to form on the coating. At 1100°C the peaks for LSCF were stronger. In Figure.22, XRD analysis of the sample C15, which was heat treated at 1300°C, is given. Peaks for

LSCF-6482 were observed along with stronger peaks from the CeO₂ from the substrate (see Table 5 and Figure 22). The high temperature post heat treatment transformed some of the phases and produced a dense microstructure as shown in Figure 4.16a.

The XRD chart showed that the LSCF layer was not glassy but dense and crystalline. Figure 23 shows the XRD analysis result for sample Z1, which was made to produce LSCF coating on TZ-3Y substrate. But the post heat treatment temperature was 900°C and some of the salts in the coating dissociated to produce an intermediate compound $\text{La}_{0.5}\text{Sr}_{0.5}(\text{CoO}_3)$. Apparently iron was not yet accommodated in the structure to enable formation of LSCF. When the same sample was heated to 1300°C after coating LSCF-7337 ($\text{La}_{0.7}\text{Sr}_{0.3}\text{Co}_{0.3}\text{Fe}_{0.7}$) as well as SZO (SrZrO₃), LZO (La₂(Zr₂O₇)) and LaO were observed in Figure 24. Notice that the LSCF was still not the intended 6482 composition but a La and Fe-rich phase formed instead. While there was no iron in Figure.23 in the LSC composition at 900°C heated sample, sample Z3 in Figure 25 was able to produce an Fe-rich LSCF compound. Sample Z1, for example, contained CeO₂ and LSC phases without much iron.

When the same sample was heated to 1300°C (sample Z3) iron took part in the reaction and LSCF was identified (Figure 24). Another significant observation from Figure 24 is that zirconia stole some of the La and Sr and therefore an LSCF compound with 7337 stoichiometry formed instead of the desired 6482 compound. The substrate CGO, on the other hand, was able to produce complete LSCF-6482 stoichiometry after 1300°C heat treatment (sample C15). A lower temperature heat treatment was insufficient to achieve the desired stoichiometry (sample C13).

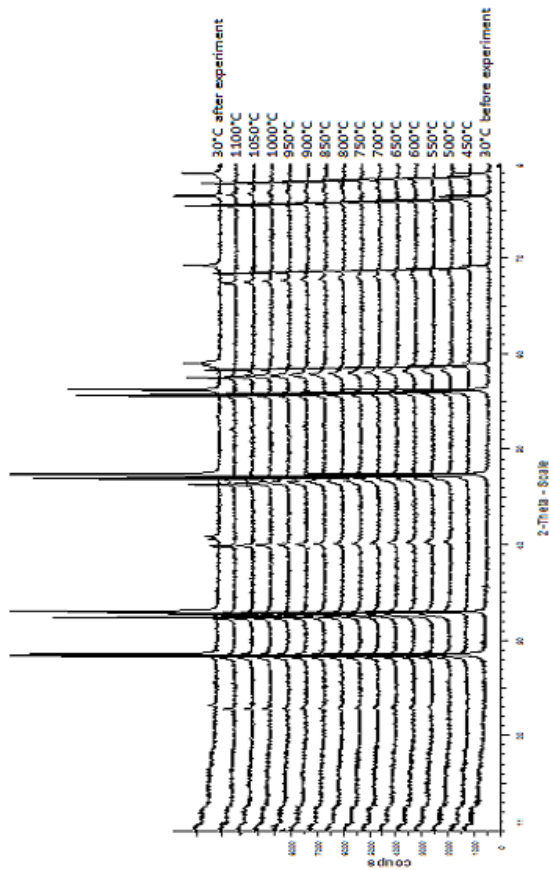


Figure 21. HTXRD result of $\text{La}_{0.6}\text{Sr}_{0.4}\text{Co}_{0.8}\text{Fe}_{0.2}\text{O}_{3-\delta}$ on CGO. This sample was prepared under the same conditions with C13 but without the post heat treatment

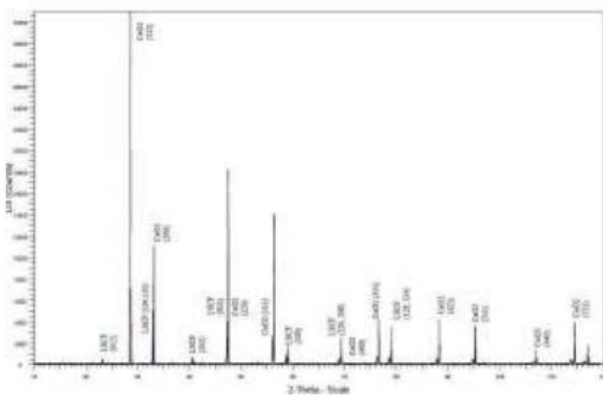


Figure 22. XRD chart for sample C15

Figures 25 and 26 show high temperature X-ray analysis of samples prepared under the same conditions with Z1 and Z3. Again the peaks for the substrate ZrO_2 shifted to the left due to lattice expansion upon heating. Starting with 550°C and

higher formation of compounds like LSC and LSCF were observed following decomposition of salts in the coating. The sample heated at 1300°C showed similar XRD pattern. In Figures 27 and 28, XRD analysis results of the $\text{La}_{0.6}\text{Sr}_{0.4}\text{Co}_{0.2}\text{Fe}_{0.8}\text{O}_3$ (LSCF-6428) coating on

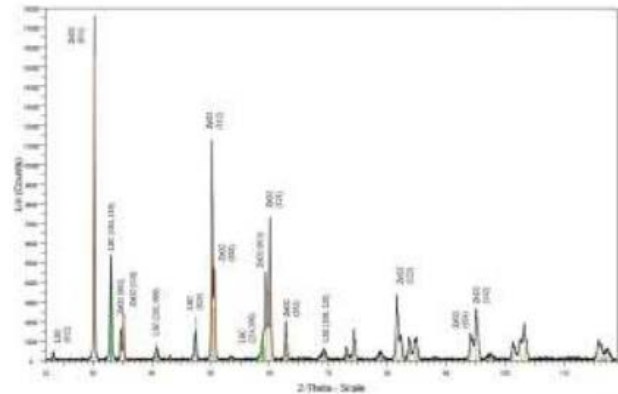


Figure 23. XRD chart for sample Z1

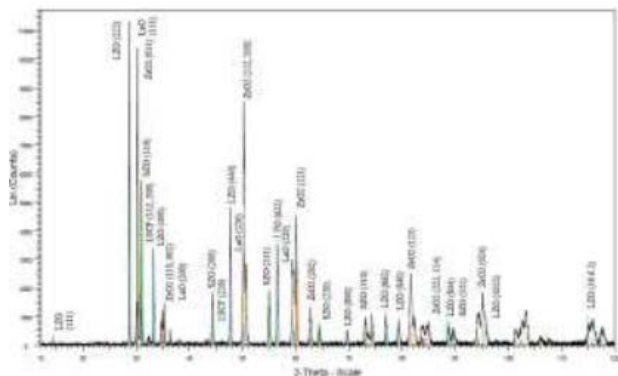


Figure 24. XRD chart for sample Z3

CGO substrate are shown. The samples were heat-treated at 900°C and 1300°C, respectively. At 900°C, CeO_2 and $\text{Sr}_{0.6}\text{La}_{0.4}\text{FeO}_3$ (SLF) compounds were found in sample C16. In addition to these compounds, $\text{La}_{0.6}\text{Sr}_{0.4}\text{CoO}_3$ compound was observed at 1300°C in sample C18. Although $\text{La}_{0.6}\text{Sr}_{0.4}\text{Co}_{0.8}\text{Fe}_{0.2}\text{O}_3$ (LSCF-6482) composition can be formed on CGO substrate, for example C15 sample, $\text{La}_{0.6}\text{Sr}_{0.4}\text{Co}_{0.2}\text{Fe}_{0.8}\text{O}_3$ (LSCF-6428) did not form on the same substrate for any of the temperatures. Iron ions were unable to get into the LSCF structure, but formed a separate iron-containing compound of SLF instead.

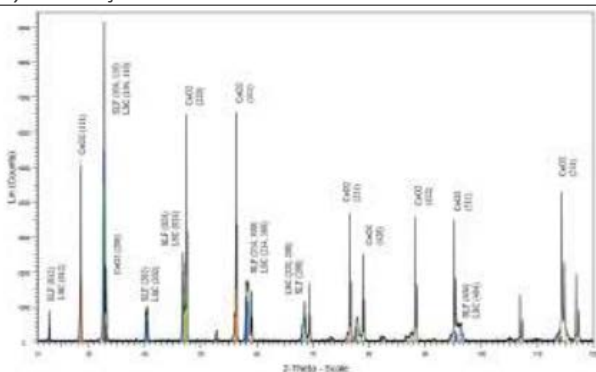


Figure 28. XRD chart for sample C18

4. Conclusion

LSCF coating on CGO and TZ-3Y substrates was successfully accomplished. Initially, a solution with the correct stoichiometry for $\text{La}_{0.6}\text{Sr}_{0.4}\text{Co}_{0.8}\text{Fe}_{0.2}\text{O}_{3-\delta}$ (LSCF-6482) was prepared by dissolving mixtures of salts of $\text{La}(\text{NO}_3)_3 \cdot 6\text{H}_2\text{O}$, $\text{SrCl}_2 \cdot 6\text{H}_2\text{O}$, $\text{Fe}(\text{NO}_3)_3 \cdot 9\text{H}_2\text{O}$, $\text{Co}(\text{NO}_3)_2 \cdot 6\text{H}_2\text{O}$ in ethanol-water or butyl carbitol-ethanol solvents. Different compositions of solvent mixtures were tested. Electrical conductivities of the solutions were also measured to make sure that the salts were completely dissolved. An ESD (electrostatic spray deposition) setup was used to spray-coat the LSCF solutions on heated substrates. The ceramic samples were found to be successfully coated with good reticulated structure in most of the samples. Especially the samples coated at 15 mm distance, 0.7 ml/h of flow rate and 250°C of substrate heating temperature were observed to be coated best. The coating layer was continuous over the surface of the substrate with a minimum thickness of 1 μm when they were post heat treated at 900°C. The substrate type did not make any difference on the coating structure. When this heat treatment temperature was increased to 1300°C the coating was found to have a fully dense structure with no porosity. This dense structure was not amorphous but was crystalline as determined by XRD to be largely composed of crystals of LSCF-6482. TZ-3Y was found to react with the coating and to modify its composition to deviate from LSCF-6482. CGO substrate appeared to be better in terms of compatibility with the coating during thermal treatment step. Electrical measurements need to

be done to reach conclusions about the potential service performance of the system. It is suggested that electrical conductivity measurements be done on the samples. Another topic for potential future study is to study interface reactions between prepared LSCF coating and the substrate on furnace heated samples instead of ESD coated samples. Thermodynamic assessment of potential reactions between substrate and coating must be done to obtain predictive information about the suitability of different substrate and coating systems.

Acknowledgements

The authors would like to thank the Laboratoire d'Electrochimie et de Physicochimie des Matériaux et des Interfaces (LEPMI) Center of Material at Université Joseph Fourier Grenoble, France, for the facilities ESD, SEM, XRD and DTA/TGA measurements and technical support. We also would like to thank to Daniel Marinha, Said Obbade, Elisabeth Djurado for their help, patience and friendship during the laboratory works.

References

- Chen, C.H., Kelder, E.M., Van der Put, P.J.J.M. and Schoonman, J. 1998. Thin Films Components For Lithium Ion Batteries. Ph.D. Delft University of Technology, Netherlands, Electrochemical Society Proceedings, 96, 14, 43-57.
- EG&G Technical Services, 2004. Inc. Fuel Cell Handbook, 7th ed.; U.S. Department of Energy Office of Fossil Energy National Energy Technology Laboratory, West Virginia, 2004.
- Hoogers, G., 2003. Fuel Cell Technology Handbook, 2nd.; CRC Press, 1-332.
- <http://www.ecn.nl> (29.06.2010).
- Huijmans, J.P.P., 2001. Ceramics In Solid Oxide Fuel Cells. Solid State & Materials Science, 5, 317-323.
- Marinha, D., Rossignol, C. and Djurado, E. 2009, Influence of Electro spraying Parameters on the Microstructure of $\text{La}_{0.6}\text{Sr}_{0.4}\text{Co}_{0.2}\text{Fe}_{0.8}\text{O}_{3-\delta}$ Films for SOFCs. Journal of Solid State Chemistry, 182, 1742-1748.
- Minh, N.Q. and Takahashi, T., 1995. Science and Technology of Ceramic Fuel Cells. Elsevier Science, 1-379.
- Nguyen, T. and Djurado, E., 2001, Deposition and

Characterization of Nanocrystalline Tetragonal Zirconia Films Using Electrostatic Spray Deposition, *Solid State Ionics*, 138, 191-197.

Steele, B.C.H., 2000. Materials for IT-SOFC Stacks 35 Years R&D: The Inevitability of Gradualness, *Solid State Ionics*, 134, 3-20.

Taniguchi, I., Landschoot, R.C.V. and Schoonman, J., 2003, Fabrication of La_{1-x}Sr_xCo_{1-y}Fe_yO₃ Thin Films by Electrostatic Spray Deposition. *Solid State Ionics*, 156, 1-13.

Tietz, F., Mai, A. and Stöver, D. 2008. From Powder Properties to Fuel Cell Performance A Holistic Approach for SOFC Cathode Development, *Solid State Ionics*, 179, 1509-1515.

Wilhelm, O., Pratsinis, S.E., Perednis, D. and Gauckler, L.J., 2005. Electrostatic Spray Deposition of Yttria Stabilized Zirconia Films. *Thin Solid Films*, 479, 121-129.

Yamamoto, O., Arati, Y., Takeda, Y., Imanishi, N., Mizutani, Y., Kawai, M. and Nakamura, Y., 1995, Electrical Conductivity of Stabilized Zirconia with Ytterbia and Scandia *Solid State Ionics*, 79, 137-142.